Evidence for topological behavior in superconducting Cu_xZrTe_{2-y}

A. J. S. Machado,[1] N. P. Baptista,[1] B. S. de Lima,[1] N. Chaia,[1] T. W. Grant,[1,2] L. E. Corrêa,[1] S. T. Renosto,[1] A. C. Scaramussa,[1] R. F. Jardim,[3] M. S. Torikachvili,[4] J. Albino Aguiar,[5] O. C. Cigarroa,[1] L. T. F. Eleno,[1] and Z. Fisk[2]

[1]*Universidade de São Paulo Escola de Engenharia de Lorena, Lorena, Brazil*

[2]*University of California, Irvine, California 92697, USA*

[3]*Universidade de São Paulo, São Paulo, Brazil*

[4]*San Diego State University, San Diego, California 92182, USA*

[5]*Universidade Federal de Pernambuco (UFPE), Recife, Brazil*

(Received 17 October 2016; revised manuscript received 17 February 2017; published 4 April 2017)

We present structural, magnetic, electrical, thermal transport, Hall coefficient, and pressure-dependent resistivity measurements on Cu_xZrTe_{2-y} compounds with $x = 0.05$, 0.1, 0.15, 0.2, and 0.3, and y varied between $0 \leqslant y \leqslant 0.8$. In order to calculate the ground state, *ab initio* calculations of the electronic structure of these materials were performed. Our results show that copper intercalation in $ZrTe_2$ induces superconductivity in the $ZrTe_2$ system. For the $Cu_{0.3}ZrTe_{1.2}$ sample, Hall and Seebeck coefficient measurements show that the system is predominantly negatively charged with carrier density close to $10^{19}\,cm^{-3}$. The temperature dependence of the Hall coefficient, the Seebeck coefficient, and the lower critical field indicates that this material presents multiband character. Pressure-dependent resistivity vs temperature measurements reveal that while the normal-state resistivity decreases with increasing applied pressure, the superconducting transition temperature is completely insensitive to the applied pressure (for pressure in the range 0–1.3 GPa). This suggests that the Fermi gas is intrinsically degenerate under very high pressure, and therefore does not change much with varying external pressure. Finally the band structure calculation shows a dispersion curve containing a bulk three-dimensional Dirac conelike feature at the L point in the Brillouin zone, which is gapless in the absence of spin-orbit coupling, but develops a gap when this coupling is considered. Altogether, the results indicate that the superconducting compound Cu_xZrTe_{2-y} presents a signature of multiband behavior and may possibly be a new example of a topological superconductor.

DOI: 10.1103/PhysRevB.95.144505

I. INTRODUCTION

Layered transition-metal dichalcogenide compounds with general composition MX_2 (M = transition metal, and X = S, Se, or Te) display a large variety of physical properties. Some examples are $NbSe_2$, TaS_2, and $TaSe_2$, which have been thoroughly studied for their rich electronic properties [1–4]. In these compounds, the transition-metal sheet is sandwiched between two similar chalcogen sheets. The interaction between these three-layer units has a van der Waals nature and hence is very weak. This particular characteristic creates a perfect environment for elemental intercalation that frequently results in significant modification of the properties [5–8].

This change in behavior upon intercalation can be explained in terms of charge transfer between the intercalated (atoms or molecules) and the host MX_2 layers. While the band structure remains unaltered upon intercalation, the density of states at the Fermi level changes, as described by the rigid-band model (RBM). The validity of this model is supported by photoemission experiments in various intercalated MX_2 compounds [9–12]. However, recent results with the intercalation of an organic molecule $[(pyridine)_{1/2}]TaS_2$, and the alkaline metals Na and Cs intercalated in 2H-TaS_2 and VSe_2, suggest that the changes induced by intercalation were more extensive than that expected by the RBM [13–16]. Some reports suggest that charge-density wave and superconductivity are distinctive quantum orders which can emerge from Fermi surface instabilities that frequently can be tuned upon intercalation [17–28].

The objective of the present work is to investigate the properties of $ZrTe_2$, which crystallizes in the layered CdI_2-type structure (space group $P\bar{3}m1$). $ZrTe_2$ can be formed in a large stoichiometry range in the Zr-Te binary system, i.e., the phase (existing with a deficiency of Zr and/or Te within the same prototype structure) can accommodate a fairly wide range of deficiency of either element. In this paper we present evidence that copper intercalation in $ZrTe_2$ induces superconductivity with the signature of multiband behavior, and that it may possibly be a new example of a topological superconductor.

II. EXPERIMENTAL PROCEDURE

Polycrystalline samples with Cu_xZrTe_{2-y} compositions were prepared from the stoichiometric mixture of high-purity powders of Zr, Cu, and Te, with $x = 0.05$, 0.1, 0.15, 0.2, and 0.3, and $0 \leqslant y \leqslant 0.8$. The stoichiometric mixtures were ground thoroughly and pressed into pellets of 8.0 mm diameter and approximately 1.5 mm thickness. The pellets were encapsulated in quartz tubes under argon and heated at 850 °C for 48 h. After this heat treatment the samples were reground, pressed, and sealed in quartz again under the same conditions, soaked at 1000 °C for an additional 48 h, and then quenched in ice water, to avoid the formation of low-temperature phases (typically the $ZrTe_3$ phase). All samples were characterized by x-ray diffraction (XRD) in a PANalytical diffractometer (model Empyrean), with detector PIXcel^{3D} using Cu $K\alpha$ radiation. Magnetic, electric, thermal, and Hall characterizations were made using a Quantum Design Physical Property Measurement System (PPMS). The Hall coefficient and carrier density were estimated using the van der

Pauw technique [29]. The thermoelectric potential was measured using the PPMS's thermal transport option. The pressure dependence of the electrical resistivity of $Cu_{0.3}ZrTe_{1.2}$ in pressures up to 1.3 GPa was determined using a piston-cylinder self-locking cell, using silicone oil as the pressure-transmitting medium. The pressure at low temperatures was determined from the superconducting (SC) transition temperature of pure Pb.

III. CALCULATION METHODS

In order to obtain the ground-state electronic structure for the compound Cu_xZrTe_2, *ab initio* calculations were performed using the WIEN2K computational code [30] following the full-potential linear augmented plane wave plus local orbitals method [31], in the framework of the Kohn-Sham scheme [32] within the density functional theory [33]. Exchange and correlation effects were treated using the generalized gradient approximation using the parametrization due to Perdew *et al.* [34], taking relativistic corrections and spin-orbit coupling into account. Muffin-tin radii (R_{MT}) were taken as 0.106 nm for all nuclei, with a product $R_{MT}K_{max} = 9.0$, where K_{max} is related to the basis set size. We used 10 000 k points in the first Brillouin zone. All lattice parameters and atomic positions were relaxed in order to guarantee a convergence in total energy within 10^{-5} Ry ($=13.6 \times 10^{-5}$ eV) in the self-consistent procedure. It should be noted that we assumed that all Cu crystallographic positions were filled by copper nuclei, so that the stoichiometry of the calculated compound is $CuZrTe_2$.

IV. RESULTS AND DISCUSSION

The equilibrium phase diagram of the Zr-Te binary system shows six binary compounds. Among them, the $ZrTe_2$ is an equilibrium phase with stoichiometry composition between 33 and 43 at. % zirconium [35]. $ZrTe_2$ crystallizes with hexagonal CdI_2-type structure (space group $P\bar{3}m1$) [36], shown schematically in the inset of Fig. 1, with Cu atoms already intercalated into the structure of the compound. The zirconium atoms occupy the (0,0,0) atomic positions, while the tellurium atoms occupy the (1/3,2/3,1/4) positions, with the layers in the stacking sequence Zr-Te-Te-Zr. The weak van der Waals bonds between the Te layers are amenable to an interlayer intercalation. In this work we studied the effect of copper intercalation. Figure 1 shows the Rietveld refinement for experimental x-ray diffraction data of a $Cu_{0.3}ZrTe_2$ sample. The refinement was carried out using the POWDERCELL [37], VESTA crystallography [38], and EXPGUI-GSAS [39] codes.

The agreement between experimental and simulated spectra is excellent and the refinement provided error parameters such as goodness-of-fit (χ^2) and weighted-profile reliability factor (R_{wp}) of 1.61% and 8.71%, respectively. The refinement demonstrates that the copper atoms used in the sample preparation were incorporated in the $ZrTe_2$ structure. The inset in Fig. 1 shows a schematic diagram of the probable sites where the copper intercalation may happen. The XRD structural refinement yielded for the lattice parameters of the intercalated compound $Cu_{0.3}ZrTe_2$ the values $a = 3.959$ Å and $c = 6.656$ Å, slightly higher than the values for pure $ZrTe_2$, which is consistent with intercalation.

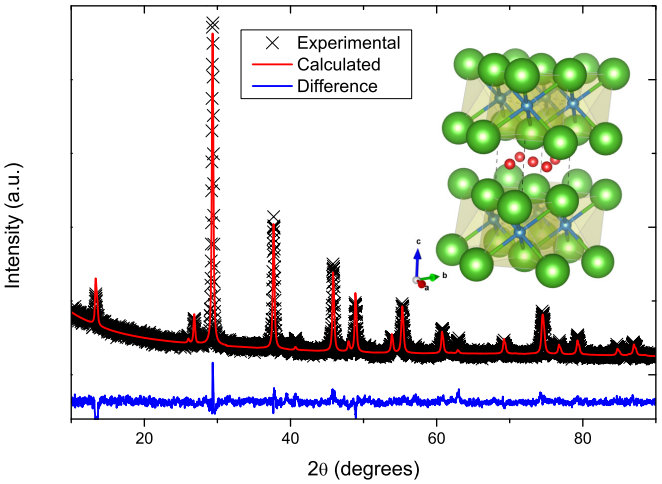

FIG. 1. X-ray diffraction data and Rietveld refinement for a sample with composition of $Cu_{0.3}ZrTe_2$. Blue spheres represent Zr ions, green spheres represent Te ions, and red spheres represent Cu ions.

Figure 2 exhibits magnetization and resistivity data for a sample with nominal composition of $Cu_{0.3}ZrTe_{1.2}$. A diamagnetic signal, shown in Fig. 2(a) at 2 K with an applied magnetic

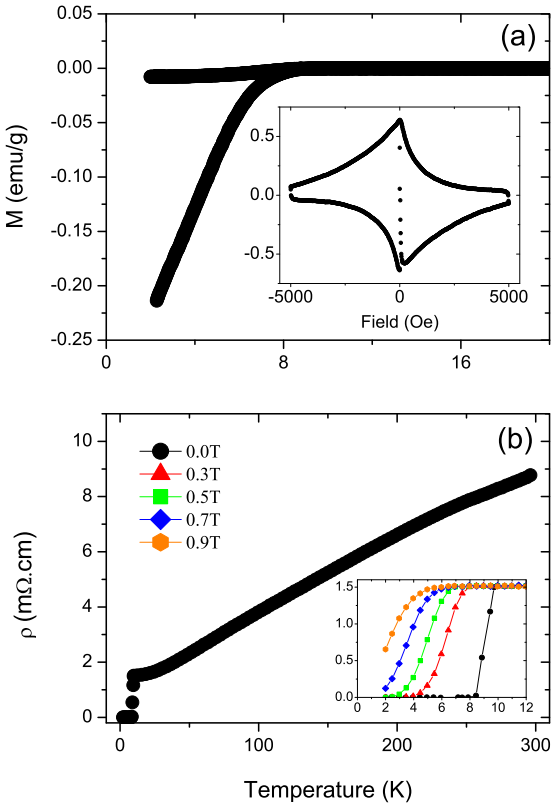

FIG. 2. (a) Magnetization and (b) electrical resistivity as function of temperature for $Cu_{0.3}ZrTe_{1.2}$. The upper inset presents M vs H at 2 K and the lower inset shows the SC transition for different external fields applied.

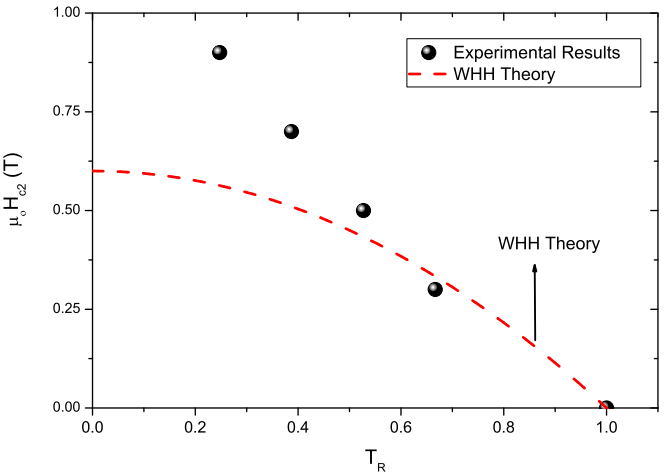

FIG. 3. H_{c2} phase diagram built from magnetoresistance displayed in the lower inset of Fig. 2, showing the strong deviation from usual WHH behavior represented by the dashed red line.

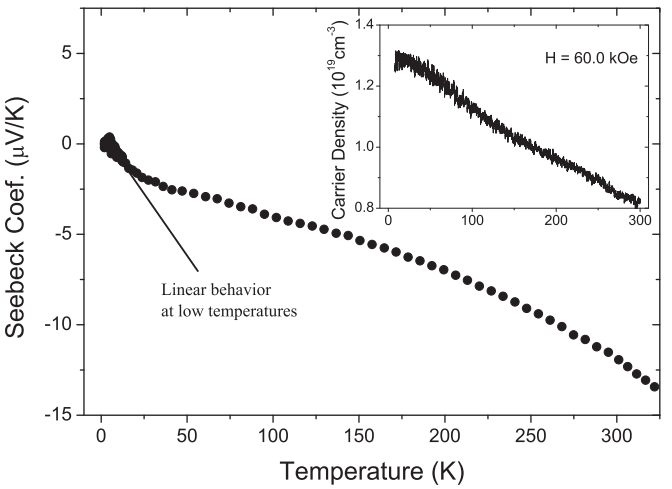

FIG. 4. Temperature dependence of Seebeck coefficient for $Cu_{0.3}ZeTe_{1.2}$ sample. The inset presents carrier density as a function of temperature extracted from the Hall coefficient measured at 6.0 T.

field of 25 Oe strongly suggests bulk superconductivity at critical temperature $T_c \approx 9.7$ K. Magnetization versus applied magnetic field at 2.0 K is shown in the upper inset of Fig. 2, and it is possible to observe a type-II superconducting response. This data is in agreement with electrical resistivity data, shown in Fig. 2(b), in which it is possible to observe a metal-like behavior down to 9.7 K. At this point we observe a sharp superconducting transition ($\Delta T_c \sim 1.2$ K) that has the T_c suppressed with applied magnetic field. Samples with other compositions were also prepared. $Cu_{0.3}ZrTe_2$ also shows the superconducting transition close to 10.0 K. However, the superconducting volume is small (data not shown) even though the x-ray diffraction pattern reveals a single-phase sample. The small magnitude of the magnetic shielding suggests that the superconductivity in this sample is not bulk. Our investigations were conducted for several Cu and Te compositions and the best results were found in the Te-deficient samples with Cu content of $x = 0.3$. We point out the fact that pure $ZrTe_{1.2}$ samples, with Te deficiency with respect to the $ZrTe_2$ composition, do not exhibit a superconducting transition, showing instead a metal-insulator transition (data not shown). This is an indication that the superconductivity is triggered by the presence of the Cu layers.

Figure 3 shows the upper critical field H_{c2} phase diagram for samples with composition of $Cu_{0.3}ZrTe_{1.2}$. The H_{c2} vs T_R (where T_R is the reduced temperature defined by T/T_c) phase diagram was constructed using the superconducting transition midpoint from the resistivity measurement shown in Fig. 2(b). In general, in the dirty limit most authors use the Werthamer-Helfand-Hohenberg (WHH) formula [40] given by

$$\mu_0 H_c(0) = -0.693 T_c \left(\frac{dH}{dT}\right)_{T_c}. \quad (1)$$

Using the derivative close to T_c in Eq. (1) allows us to estimate the upper critical field at zero Kelvin. However, a strong deviation from the expected WHH theory (dashed red line) behavior can be clearly observed in Fig. 3. This kind of deviation could suggest a multiband manifestation in this material, similar to what occurs in many materials that are recognized as multiband such as MgB_2, $LaNiC_2$, or $ThCoC_2$ [41–43].

The Seebeck coefficient does not depend on the electron effective mass, and with this goal we did the measurements of this important parameter as a function of temperature (2–300 K) for a $Cu_{0.3}ZrTe_{1.2}$ sample, as shown in Fig. 4. The thermoelectric potential drops to zero near T_c, consistent with a bulk superconducting state observed in Fig. 2. The predominance of n-type carrier is consistent with the Hall effect measurement, as shown in the inset of Fig. 4. The Hall effect measurement as a function of temperature shows a negative charge-carrier density decreasing linearly with increasing temperature, which is an unusual behavior for a metallic material. The linear dependence in the Seebeck coefficient at low temperature also allows an estimation of the carrier density using the S/T rate, and is consistent with the Hall effect measurements. This set of results (Seebeck and Hall effects) demonstrates that the carrier density is very low, and once again indicates the possibility of the superconductivity being due to topological effects arising from the copper doping. In contrast to the Cu-induced superconducting topological material $Cu_{0.12}Bi_2Se_3$ [27], where the Hall coefficient is independent of temperature, the linear temperature dependence of the Hall coefficient observed in $Cu_{0.3}ZrTe_{1.2}$ suggests that more than one band contributes to the Fermi surface since this behavior requires more than one relaxation time. Indeed the linear dependence of the Hall voltage on temperature is a signature of multiband behavior, which has been observed in compounds such as MgB_2, fullerenes, and some organic materials [39–43]. The obtained n values are close to 10^{19} cm^{-3}, which is much smaller than values found normally in metals.

Another unusual behavior observed in $Cu_{0.3}ZrTe_{1.2}$ compound is in the lower critical field (H_{c1}). H_{c1} can be estimated from the applied magnetic field dependence of the magnetization by determining the point of departure from linearity of the magnetization curve at low field. Thus, the

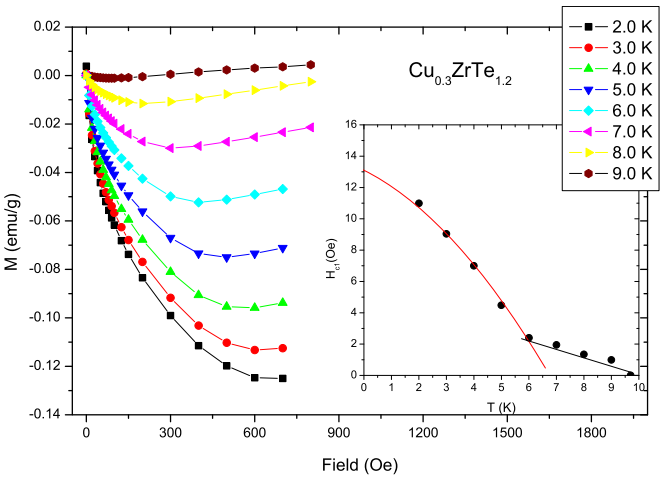

FIG. 5. M vs H for several temperatures between 2.0 and 9.0 K. The H_{c1} can be defined by the departure from linearity on the slope of this figure at each temperature. The inset shows the H_{c1} vs T phase diagram, showing an unusual behavior with a slope change close to 60% at the critical temperature.

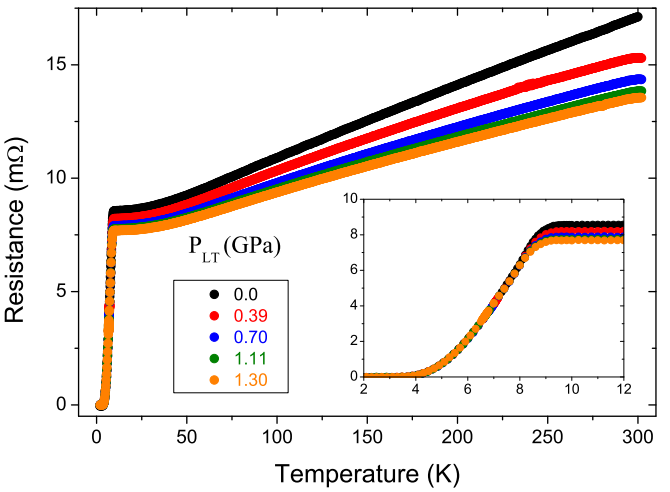

FIG. 6. R vs T under applied pressure between 0 and 13.0 kbar. As shown in the inset, the superconducting transition temperature is not affected by pressure.

dependence of the magnetization on the applied field (M vs H curves) was measured at several temperatures, as shown in Fig. 5.

It is observed that the deviation from linearity in M vs H curves occurs at magnetic fields, below ≈15 Oe. These results provide a London penetration depth estimate of about 0.5 μm, which is about 100 times larger than conventional superconductors and is consistent with the very low carrier concentration. The inset of Fig. 5 shows the temperature dependence of the lower critical field. The H_{c1} vs T phase diagram displays an unusual nonmonotonic behavior. This behavior (H_{c1} vs T) is also observed in materials that are considered multiband compounds [44–54], like in MgB_2 with holelike boron σ band and π band structure [54]. These results are also consistent with the interpretation of multiband character obtained from the carrier density in the Hall coefficient results shown in Fig. 4. These sets of results extracted from Figs. 4 and 5 are completely consistent and strongly suggest a multiband behavior in this new superconducting material.

Figure 6 shows the temperature dependence of the resistivity as a function of the applied pressure in the range of 0–1.3 GPa, for the sample with composition $Cu_{0.4}ZrTe_{1.2}$. Although presenting a slightly lower transition temperature (T_c onset near 9.0 K) and a wider superconducting transition width compared to the $Cu_{0.3}ZrTe_{1.2}$ sample, it is surprising the superconducting transition temperature T_c is completely insensitive to applied pressure while the normal-state resistivity drops noticeably with pressure. This behavior indicates that phonons are sensitive to applied external pressure. However, an explanation for why the superconducting state does not respond to applied pressure is not so obvious, but it may be that it corresponds to an intrinsically degenerate Fermi gas under very high pressures, and therefore does not change much with varying external pressure. We conclude that this kind of behavior can be intrinsic of the topological superconductivity and these results offer evidence for that.

Indeed, the band structure calculation shown in Fig. 7 reveals some interesting characteristics and suggests the presence of a topologic effect in this copper intercalated material. Figure 7(a) shows the band structure calculations for

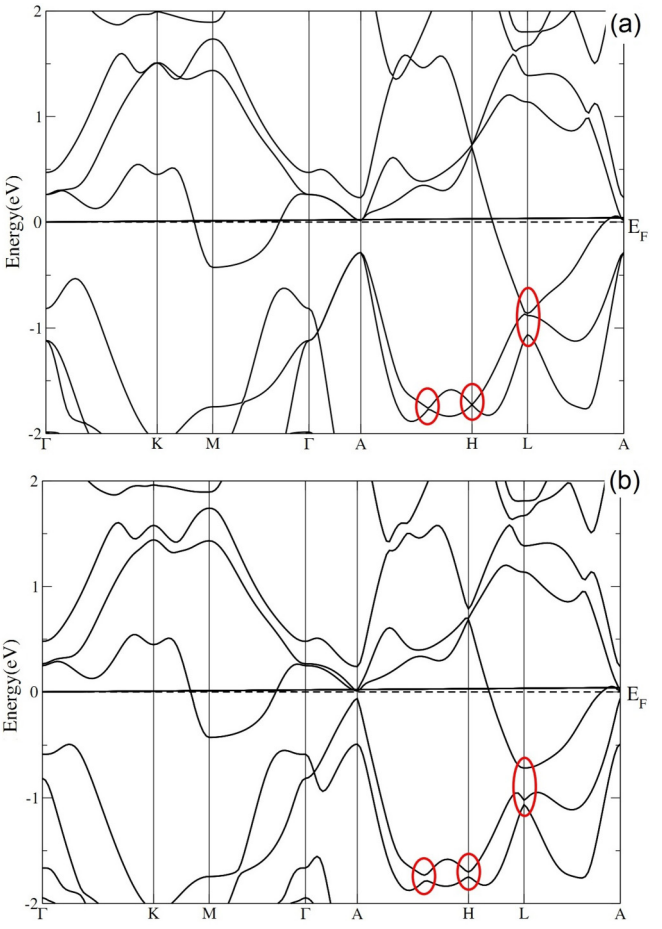

FIG. 7. (a) Band structure calculation for $Cu_xZrTe_{1.2}$ without SOC. (b) Calculated electronic structures with SOC, revealing the continuous gap opened at L when SOC is considered.

$Cu_xZrTe_{1.2}$ without spin-orbit coupling (SOC), where we can observe a dispersion curve similar to a bulk three-dimensional (3D) Dirac cone at the *L* point in the Brillouin zone, with zero gap, as well as two less-pronounced features around the *H* point (highlighted with ellipses). However, when SOC effects are considered, these features are gapped [Fig. 7(b)]. This kind of behavior also occurs in graphene at the *K* point in the Brillouin zone [55] and also in a few compounds, such as $Bi_{14}Rh_3In_9$ [56]. This signature suggests that the SOC, being topologically nontrivial, gaps this single Dirac cone at the *L* point. Besides, although the compound is metallic, there is a continuous gap around the Fermi energy when SOC is considered. Indeed similar behavior can be observed in other topological materials such as the noncentrosymmetric superconductor $PbTaSe_2$ [57]. Taken together with the experimental results for applied pressures, discussed above, the band structure calculations strongly suggest that Cu_xZrTe_{2-y} can represent a new example of a superconductor with nontrivial topological effects.

V. CONCLUSION

In this work we showed results about a systematic study of the properties of the $Cu_xZrTe_{1.2}$ compound, which indicate that copper intercalation in the $ZrTe_2$ host induces a superconducting behavior with a critical superconducting temperature close to 9.7 K, as revealed through magnetization and resistivity measurements. The charge-carrier density varies with temperature suggesting multiband behavior in this new material. The charge-carrier density is low (10^{19} cm^{-3}), which suggests that this material is an *n* semimetal consistent with the electronic structure calculations. These results are completely consistent with different measurement techniques such as Hall effect and Seebeck coefficient. The low charge-carrier density suggests that the observed superconducting behavior comes from topological effects, as also suggested by the band structure calculation. Indeed, the band calculation strongly points to a nontrivial topological effect revealed by the 3D Dirac conelike feature at the *L* point in the Brillouin zone. Pressure-dependent resistivity vs temperature measurements reveal that the normal-state resistivity decreases with increasing applied pressure, while the superconducting transition temperature is completely insensitive to the applied pressure (0–1.3 GPa). This suggests that the Fermi gas is intrinsically degenerate under very high pressures and therefore does not change much with varying external pressure. The set of results demonstrate that this material could be another example of a topological superconductor with multiband effect.

ACKNOWLEDGMENTS

This work was financially supported by the Brazilian research agencies CAPES, CNPq (Grants No. 302850/2014-7 and No. 443385/2014-9), and FAPESP (Grant No. 2013/16873-3).

[1] T. Valla, A. V. Fedorov, P. D. Johnson, P-A. Glans, C. McGuinness, K. E. Smith, E. Y. Andrei, and H. Berger, Phys. Rev. Lett. **92**, 086401 (2004).
[2] J. A. Wilson and A. D. Yoffe, Adv. Phys. **18**, 193 (1969).
[3] A. H. Castro Neto, Phys. Rev. Lett. **86**, 4382 (2001).
[4] J. M. E. Harper and T. H. Geballe, Phys. Lett. A **54**, 27 (1975).
[5] F. R. Gamble, J. H. Osiecki, M. Cais, and R. Pisharody, Science **174**, 493 (1971).
[6] F. Sernetz, A. Lerf, and R. Schollhorn, Mater. Res. Bull. **9**, 1597 (1974).
[7] A. Lerf, F. Sernetz, W. Biberacher, and R. Schollhorn, Mater. Res. Bull. **14**, 797 (1979).
[8] E. Morosan, H. W. Zandbergen, B. S. Dennis, J. W. G. Bos, Y. Onose, T. Klimczuk, A. P. Ramirez, N. P. Ong, and R. J. Cava, Nat. Phys. **2**, 544 (2006).
[9] H. P. Hughes and J. A. Scarfe, J. Phys.: Condens. Matter **8**, 1439 (1996).
[10] G. Y. Guo and W. Y. Liang, J. Phys. C **20**, 4315 (1987).
[11] K. Motizuki, N. Suzuki, and S. Tomishima, J. Magn. Magn. Mater. **104**, 681 (1992).
[12] P. Blaha, J. Phys.: Condens. Matter **3**, 9381 (1991).
[13] A. H. Thompson, F. R. Gamble, and R. F. Koehler, Phys. Rev. B **5**, 2811 (1972).
[14] H. E. Brauer, H. I. Starnberg, L. J. Holleboom, H. P. Hughes, and V. N. Strocov, J. Phys.: Condens. Matter **13**, 9879 (2001).
[15] H. E. Brauer, H. I. Starnberg, L. J. Holleboom, V. N. Strocov, and H. P. Hughes, Phys. Rev. B **58**, 10031 (1998).
[16] L. Fang, Y. Wang, P. Y. Zou, L. Tang, Z. Xu, H. Chen, C. Dong, L. Shan, and H. H. Wen, Phys. Rev. B **72**, 014534 (2005).
[17] D. J. Eaglesham, J. W. Steeds, and J. A. Wilson, Phys. C: Solid State Phys. **17**, L697 (1984).
[18] P. Monceau, J. Peyrard, J. Richard, and P. Molinié, Phys. Rev. Lett. **39**, 161 (1977).
[19] S. Takashashi, T. Sambongi, J. W. Brill, and W. Roark, Solid State Commun. **49**, 1031 (1984).
[20] H. Nakajima, K. Nomura, and T. Sambongi, Physica B **143**, 240 (1986).
[21] X. Zhu, H. Lei, and C. Petrovic, Phys. Rev. Lett. **106**, 246404 (2011).
[22] H. Lei, X. Zhu, and C. Petrovic, Europhys. Lett. **95**, 17011 (2011).
[23] M. Kamitani, M. S. Bahramy, R. Arita, S. Seki, T. Arima, Y. Tokura, and S. Ishiwata, Phys. Rev. B **87**, 180501 (2013).
[24] J. J. Yang, Y. J. Choi, Y. S. Oh, A. Hogan, Y. Horibe, K. Kim, B. I. Min, and S.-W. Cheong, Phys. Rev. Lett. **108**, 116402 (2012).
[25] Y. Xia, D. Qian, D. Hsieh, L. Wray, A. Pal, A. Bansil, D. Grauer, Y. S. Hor, R. J. Cava, and M. Z. Hasan, Nat. Phys. **5**, 398 (2009).
[26] Y. L. Chen *et al.*, Science **325**, 178 (2009).
[27] Y. S. Hor, A. J. Williams, J. G. Checkelsky, P. Roushan, J. Seo, Q. Xu, H. W. Zandbergen, A. Yazdani, N. P. Ong, and R. J. Cava, Phys. Rev. Lett. **104**, 057001 (2010).
[28] X.-L. Qi and S.-C. Zhang, Rev. Mod. Phys. **83**, 1057 (2011).
[29] M. S. da Luz, C. A. M. Dos Santos, C. Y. Shigue, F. J. H. De Cavalho, and A. J. S. Machado, Mater. Sci.-Pol. **27**, 569 (2009).
[30] P. Blaha, K. Schwarz, G. K. H. Madsen, D. Kvasnicka, and J. Luitz, *WIEN2k: An Augmented Plane Wave Plus Local Orbitals Program for Calculating Crystal Properties* (Karlheinz Schwarz, Tech. Univ. Wien, Austria, 2001).

[31] E. Sjöstedt, L. Nordström, and D. J. Singh, Solid State Commun. **114**, 15 (2000).
[32] W. Kohn and L. Sham, Phys. Rev. **140**, A1133 (1965).
[33] P. Hohenberg and W. Kohn, Phys. Rev. **136**, B864 (1964).
[34] J. P. Perdew, K. Burke, and M. Ernzerhof, Phys. Rev. Lett. **77**, 3865 (1996).
[35] S. Jobic, R. Brec, and J. Rouxel, J. Solid State Chem. **96**, 169 (1992).
[36] R. De Boer and E. H. P. Cordfunke, J. Alloy Comp. **259**, 115 (1997).
[37] W. Kraus and G. Nolze, J. Appl. Cryst. **29**, 301 (1996).
[38] K. Momma and F. Izumi, J. Appl. Crystallogr. **44**, 1272 (2011).
[39] B. H. Toby, J. Appl. Crystallogr. **34**, 210 (2001).
[40] N. R. Werthamer, E. Helfand, and P. C. Hohenberg, Phys. Rev. **147**, 295 (1966).
[41] T. Grant, A. J. S. Machado, D. J. Kim, and Z. Fisk, Supercond. Sci. Technol. **27**, 035004 (2014).
[42] V. Metlushko, U. Welp, A. Koshelev, I. Aranson, G. W. Crabtree, and P. C. Canfield, Phys. Rev. Lett. **79**, 1738 (1997).
[43] W. H. Lee, H. K. Zeng, Y. D. Yao, and Y. Y. Chen, Physica C **266**, 138 (1996).
[44] Li Lu, V. H. Crespi, M. S. Fuhrer, A. Zettl, and M. L. Cohen, Phys. Rev. Lett. **74**, 1637 (1995).
[45] N. Tajima, S. Sugawara, M. Tamura, Y. Nishio, and K. Kajita, J. Phys. Soc. Jpn. **75**, 051010 (2006).
[46] S. T. Renosto, H. Consoline, C. A. M. dos Santos, J. Albino Aguiar, S. G. Jung, J. Vanacken, V. V. Moshchalkov, Z. Fisk, and A. J. S. Machado, Phys. Rev. B **87**, 174502 (2013).
[47] A. J. S. Machado, L. E. Corrêa, M. S. da Luz, F. B. Santos, B. S. de Lima, S. T. Renosto, O. V. Cigarroa, M. R. Custódio, C. A. Nunes, G. C. Coelho, P. F. Rogl, P. F. S. Rosa, D. J. Kim, and Z. Fisk, Supercond. Sci. Technol. **28**, 095016 (2015).
[48] W. N. Kang, H. Jung Kim, H.-J. Kim, E.-M. Choi, K. H. P. Kim, H. S. Lee, and S.-I. Lee, Supercond. Sci. Technol. **16**, 237 (2003).
[49] J. L. Cohn, B. D. White, C. A. M. dos Santos, and J. J. Neumeier, Phys. Rev. Lett. **108**, 056604 (2012).
[50] J. L. Cohn, S. Moshfeghyeganeh, C. A. M. dos Santos, and J. J. Neumeier, Phys. Rev. Lett. **112**, 186602 (2014).
[51] J. Wang, X. Xu, N. Zhou, L. Li, X. Cao, J. Yang, Y. Li, C. Cao, J. Dai, J. Zhang, Z. Shi, B. Chen, and Z. Yang, J. Supercond. Novel Magn. **28**, 3173 (2015).
[52] S. L. Li, H. H. Wen, Z. W. Zhao, Y. M. Ni, Z. A. Ren, G. C. Che, H. P. Yang, Z. Y. Liu, and Z. X. Zhao, Phys. Rev. B **64**, 094522 (2001).
[53] I. N. Askerzade, A. Gencer, and N. Güçlü, Supercond. Sci. Technol. **15**, L13 (2002).
[54] Y. Kong, O. V. Dolgov, O. Jepsen, and O. K. Andersen, Phys. Rev. B **64**, 020501 (2001).
[55] C. L. Kane and E. J. Mele, Phys. Rev. Lett. **95**, 226801 (2005).
[56] B. Rasche *et al.*, Nat. Mater. **12**, 422 (2013).
[57] M. N. Ali, Q. D. Gibson, T. Klimczuk, and R. J. Cava, Phys. Rev. B **89**, 020505(R) (2014).